oceans

MDPI

Article

Influence of Seawater Ageing on Fracture of Carbon Fiber Reinforced Epoxy Composites for Ocean Engineering

Antoine Le Guen-Geffroy [1], Peter Davies [1,*], Pierre-Yves Le Gac [1] and Bertrand Habert [2]

[1] IFREMER Centre Bretagne, Marine Structures Laboratory, 29280 Plouzané, France; leguengeffroy.antoine@gmail.com (A.L.G.-G.); Pierre.Yves.Le.Gac@ifremer.fr (P.-Y.L.G.)
[2] Direction Générale de l'Armement, IP/MCM/PMA, PC62, 60 boulevard du Général Valin, 75015 Paris, France; bertrand.habert@intradef.gouv.fr
* Correspondence: peter.davies@ifremer.fr

Received: 29 August 2020; Accepted: 22 September 2020; Published: 27 September 2020

Abstract: Carbon fiber reinforced composite materials are finding new applications in highly loaded marine structures such as tidal turbine blades and marine propellers. Such applications require long-term damage resistance while being subjected to continuous seawater immersion. However, few data exist on which to base material selection and design. This paper provides a set of results from interlaminar fracture tests on specimens before and after seawater ageing. The focus is on delamination as this is the main failure mechanism for laminated composites under out-of-plane loading. Results show that there are two contributions to changes in fracture toughness during an accelerated wet ageing program: effects due to water and effects due to physical ageing. These are identified and it is shown that this composite retains over 70% of its initial fracture properties even for the worst case examined.

Keywords: composite; delamination; seawater; immersion; ageing

1. Introduction

Fiber reinforced composites are widely used in the marine industry [1,2]. Glass fiber reinforced polyesters have been used in pleasure boat and military vessel construction for over 50 years, but higher performance carbon fiber reinforced composites are finding increasing applications. These include racing yachts [3], offshore applications [4,5] and marine renewable energy structures. The latter include tidal turbine blades [6], up to 10 m long, and the latest generation of offshore wind turbine blades, over 100 m long [7]. These must perform under severe loading conditions while keeping costs low. As a result, there is increasing interest in the long-term behavior of carbon fiber composites produced by non-aerospace manufacturing routes; infusion and low pressure injection methods are of particular interest.

Despite exceptional in-plane properties, an inherent weakness of laminated composites is their sensitivity to interlaminar crack propagation or delamination due to out-of-plane loading. This has been the subject of a large number of papers since the 1970s [8], and specific experimental techniques have been developed to characterize the resistance to interlaminar fracture [9]. Mode I tests (crack opening under tensile loads) were developed first, and an ISO standard procedure was agreed in the late 1990s [10]. Mode II loading (in-plane shear) is more difficult to apply and various test configurations have been proposed [11,12], with the end loaded split (ELS) test method now an ISO standard [13]. It is also important to be able to characterize the interactions between mode I and mode II so various mixed mode loading tests have been developed. The most popular uses the mixed mode bending

(MMB) set-up, a specially designed fixture allowing different combinations of mode I and mode II to be applied by changing the fixture loading arm geometry [14]. This is an ASTM standard [15]. The output values from these tests are critical strain energy release rates, G_c, which quantify the energy necessary to either initiate or propagate delaminations. Originally used to compare materials on a consistent basis, they have become more useful in recent years as modeling techniques have been developed which use these values; in particular, cohesive zone methods (CZM) require G_c input values [16,17].

The main particularity of marine applications is temporary or permanent exposure to seawater. Many polymers are sensitive to moisture so the influence of seawater on all matrix dominated composite properties needs to be studied. For laminated composites with fibers aligned in the 0° direction, this includes off-axis tension, axial and off-axis compression, in-plane shear and all the through-thickness properties. The latter are particularly difficult to measure as laminated composites are usually quite thin and, in many cases, only the apparent interlaminar shear (ILSS) can be obtained, using short beam shear specimens (ASTM D2344). An alternative approach is to test specimens with predefined defects, thin films which are implanted during manufacture at the specimen mid-thickness. These can then be subjected to different loading types in order to measure fracture energies or critical strain energy release rates, G_c.

The resistance to interlaminar crack propagation is one of the matrix and fiber/matrix interface dominated properties which would be expected to be affected by water ingress. There have been a number of previous studies of the influence of water on delamination toughness, but the majority were focused on glass reinforced composites as this was the preferred reinforcement for marine applications. Marom summarized early work, stating that the short-term effect of water is to increase fracture toughness (plasticization), while in the long term, a deterioration effect will prevail (hydrolysis, fiber/matrix debonding) [18]. One of the aims of durability studies is to establish when this transition occurs.

Due to the more limited use of carbon composites in marine applications in the past compared to aerospace structures, there are considerably fewer papers on the delamination in water of these materials. Table 1 shows a brief overview of some results published over the last 40 years. These results concern carbon fiber reinforced epoxies and PolyEtherEtherKetone (PEEK) composites. The latter is a highly durable semi-crystalline thermoplastic.

Table 1. Previous work on the influence of wet ageing on interlaminar fracture of carbon reinforced composites.

Loading Mode	Material	Ageing Condition. Starter Crack Type	Influence of Water on Fracture Toughness	Reference
I (Double Torsion)	Carbon/Epoxy	Water 70 °C. Saw cut + razor	No effect	Thomson and Broutman, 1982 [19]
I/II	Carbon/Epoxy	50% RH, Wet. PTFE film	G_c↑ for mode I dominated No effect on G_c for shear dominated tests	Russell and Street, 1985 [20]
I, II	Carbon/Epoxy	50% RH, Wet. Mode I precrack	G_{Ic}↑, G_{IIc}↓ for wet	Garg and Ishai, 1985 [21]
I, II	Carbon/Epoxy, Carbon/PEEK	Water 22, 77, 100 °C Unaged, half-saturated, fully saturated. Foil film starter	Epoxy: G_{Ic}↑, G_{IIc}↓ PEEK: G_{Ic} no effect, G_{IIc}↓	Selzer and Friedrich, 1995 [22]
II	Carbon/Epoxy	Various RH conditions. Film	G_{IIc} ↓	Zhao, Gaedke, 1996 [23]
	Carbon/Epoxy	Dry, 50% RH, Wet Precrack	$G_{Ic\ initiation}$ no effect, $G_{Ic\ propagation}$ ↓ for wet G_{IIc} ↓ for wet	Chou I, 1998 [24]
I, II, I/II	Carbon/Epoxy	Moisture saturated. Polyimide film	G_{Ic} no effect, G_c mixed and mode II ↓ for wet	Asp, 1998 [25]
II	Carbon/Epoxy	Saturated distilled water. Film and precrack	G_{IIc} ↓ for wet	Landry et al., 2012 [26]
I	Carbon/Toughened epoxy adhesively bonded	Fresh and sea water, 70, 82 °C. Precrack	G_{Ic}↓	Couture, 2013 [27]
I/II	Carbon/Epoxy	Saturated distilled water 70 °C. Precrack	G_{Ic} ↑ $G_{I/IIc}$ ↓ for wet	LeBlanc et al., 2015 [28]

For mode I fracture, both increases and decreases in G_{Ic} after water saturation have been reported, while the effect of water absorption on the mode II and mixed mode I and II tends to reduce fracture toughness. The majority of the previous work in this area has been limited to either pure mode I or mode II loading; to the authors' knowledge, there have been very few studies in which the effects of natural seawater ageing on carbon/epoxy marine composites have been studied over the full range of mode I, mode II and mixed mode I/II loading. This is the aim of the present work.

2. Materials

The composite material studied here is a carbon fiber reinforced epoxy. Both fibers and matrix are commercially available products. The epoxy resin pre-polymers are diglycidyl ether of bisphenol F (DGEBF, ≥50%), diglycidyl ether of bisphenol A (DGEBA, ≥10%) and 1,6 hexa diglycidyl ether (≥10%). This epoxy resin is commercialized by the French manufacturer Sicomin® under the SR8100 product name. The hardener was also supplied by Sicomin®, reference SD4772. This amine-based hardener is designed for manufacturing of thick composite parts under anaerobic processes such as resin transfer molding (RTM) and infusion processes. The carbon fibers used were T700 Torayca® 12 K, 1600 tex, standard modulus unidirectional reinforcement. For both ease of handling and ease of resin impregnation, these were woven in the perpendicular direction with 68 tex glass fibers, representing a 13 to 590 glass to carbon weight ratio, resulting in a mass per unit area of 603 g/m^2.

Six-ply thick 500 × 500 mm^2, unidirectional composite plates were manufactured using the vacuum infusion process, of thickness 3.4 ± 0.1 mm. In order to perform fracture tests, a 12 µm thick by 80 mm wide sheet of polytetrafluoroethylene (PFTE) was placed at mid-thickness at each side of the plate perpendicular to the carbon fiber direction before infusion.

The composites plates were cured at ambient temperature for 24 h and post-cured for 8 h at 80 °C, followed by a post-cure of 2 h at 120°C. This final cure was necessary to completely cure and stabilize the resin, to prevent any residual curing during seawater ageing. Using TGA (thermogravimetric analysis under a nitrogen atmosphere) and a helium pycnometer to measure density, fiber and void volume ratios were calculated. The fiber volume ratio obtained from these measurements was estimated to be around 62 ± 3% with 0.8 ± 0.3% void volume ratio. The material's glass transition temperature (Tg) was measured using differential scanning calorimetry to be around 75 ± 2 °C. The overall quality of panels was checked using ultrasonic C-scan and very low attenuation was found, confirming good internal quality. Interlaminar shear strength was measured using ASTM D2344 to be 64 ± 3 MPa.

3. Experimental Methods and Data Analysis

This study focuses on the effect of long-term seawater ageing on the fracture properties of the composite. It is first necessary to establish how long the specimens need to saturate and the water temperature which can be used to accelerate water ingress. A preliminary weight gain study on the water ageing behavior of 50 × 50 × 3 mm^3 coupons showed Fickian behavior of the composite. This means that there is a stable and reversible state that is reached after a certain time, representing the fully water-saturated state. Therefore, in this study, only the fully dried, fully saturated and re-dried after full saturation states were examined. These three conditions will be referred to as unaged (fully dried), saturated (fully saturated) and saturated then dried (re-dried after full saturation).

Seawater ageing tanks were used to age composite samples. These 180 L capacity insulated tanks were filled with natural seawater pumped directly from the Brest estuary. This seawater was continuously renewed (volume replaced every 24 h). The temperature was controlled to within ±2 °C (Figure 1) and monitored continuously.

Based on results from the preliminary study, shown in Figure 2, the water temperature for specimen ageing was chosen to be 60 °C. This temperature corresponds to the highest possible accelerating temperature with respect to the material's dry Tg of 75 °C. The time to saturation of specimens at this temperature was found to be 15 weeks.

Figure 1. Seawater ageing tanks.

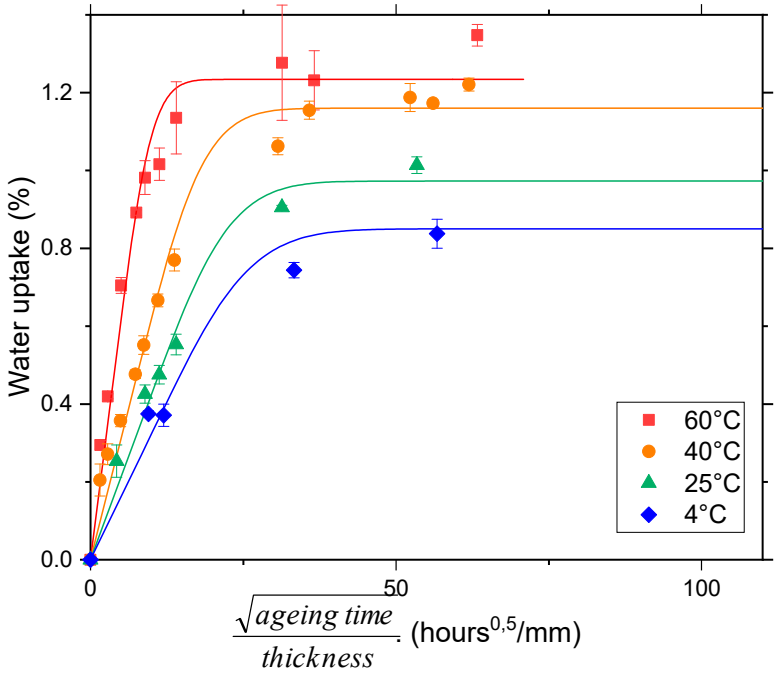

Figure 2. Preliminary water uptake results for the composite in seawater at different ageing temperatures. Lines show respective Fickian model fit. Error bars show standard deviations.

All specimens were dried prior to either testing (unaged condition) or immersion. Some mode I and mode II specimens were also dried after reaching saturation, in order to examine the reversibility of water effects, by placing them in an oven at 60 °C in desiccators, also for 15 weeks, their weight being controlled frequently in order to ensure that they were fully dried.

The interlaminar fracture properties of the composite were studied using different test methods: pure mode I delamination, pure mode II delamination and combinations of mode I and mode II loading. For all the tests, an Instron™ 5966 electromechanical test machine was used, with an Instron™ 2580-500N load cell. Controlled laboratory environment conditions of 21 ± 1 °C and 50 ± 5% relative humidity were maintained throughout the tests.

3.1. Mode I Delamination: Double Cantilever Beam (DCB)

The double cantilever beam (DCB) test method was chosen in order to test the mode I fracture toughness. These tests were performed based on the ISO 15024 standard test method [9]. Specimens were cut to 20 by 150 mm^2 dimensions. The compliance calibration (CC) data reduction method was chosen to calculate the mode I energy release rate, G_{Ic} in J/m^2, as

$$G_{Ic} = \frac{nP\delta}{2ba} \tag{1}$$

In this equation, n is the slope of the compliance logarithm log(C) versus crack length logarithm log(a). P is the load in N at the opening displacement δ in mm, b is the specimen's width in mm and a is the crack length in mm. In order to measure crack length, one of the specimen edges was painted using a white Posca® pen. This particular marker pen has many advantages such as being water-based, preventing unwanted degradation as opposed to alcohol-based paints, providing a matt finish with good opacity, thus increasing contrast with the crack, and, finally, it has no mechanical resistance so it does not affect the load measurements. A camera was placed facing the white-painted edge of the specimens and linked to a PC to record the images together with corresponding load and displacement values using a data acquisition card. The crack length value was interpolated between the initial crack length and the final crack length using the compliance. The validity of this interpolation was checked by comparing the calculated crack lengths and the optically measured crack lengths, which showed good agreement. The crosshead displacement rate was 1 mm/min, in order to follow the crack propagation accurately.

Results from all these delamination tests include both initiation and propagation values. The former can be defined by the values on the force versus displacement corresponding to either beginning of non-linearity (NL) or a 5% change in slope (5%) and using the initial starter crack length. Both were calculated here. As recommended by the standard, two cases can be identified. The first corresponds to initiation from the insert film: a short natural crack is created (5 to 10 mm from the film insert) and then the specimen is unloaded. The second initiation value is determined when the small precrack created by this first initiation cycle is reloaded. Loading is then continuous and propagation values are also calculated, using the load and displacement corresponding to each calculated crack length once the crack has started to advance along the specimen.

3.2. Mode II Delamination: Calibrated Edge Loaded Split (C-ELS)

The mode II delamination properties were evaluated using the ISO calibrated edge loaded split (C-ELS) standard test method [13]. This particular test method was chosen over other mode II configurations [11,12] due to better crack stability and longer crack propagation length. The specimen's width and length were also 20 by 150 mm^2, similar to the DCB dimensions, which facilitates specimen preparation. As with mode I tests, the loading rate was 1 mm/min. The pure mode II energy release rate, G_{IIc} in J/m^2, was calculated using the Corrected Beam Theory with the effective crack length (CBTE) data reduction method:

$$G_{IIc} = \frac{9P^2a_e^2}{4b^2h^3E_{1f}}, \text{ with} \tag{2}$$

$$a_e = \left[\frac{1}{3}\left\{2bCh^3E_{1f} - \left(L_1 + \Delta_{clamp}\right)^3\right\}\right]^{\frac{1}{3}} \tag{3}$$

In this equation, in addition to the equivalent parameters from Equation (1), a_e is the effective crack length in mm, h is the half-thickness of the specimen in mm, E_{1f} is the flexural modulus that can be determined from three point bending test or from clamp calibrating the ELS test in MPa, C is the compliance (displacement/force), L_1 is the free length, meaning the distance from the load point to the crack tip in mm, and finally, Δ_{clamp} is the clamp correction determined through the clamp calibration procedure detailed in [13].

3.3. Mode I/II Delamination: Mixed Mode Bending (MMB)

The third test procedure was also based on a standardized test, the mixed mode bending (MMB) [15]. This test method uses a special lever and base fixture that combines a three-point bending end notched flexure with a DCB test. By adjusting the position of the load point on the lever, different mode I/II combinations are obtained, as shown in Figure 3.

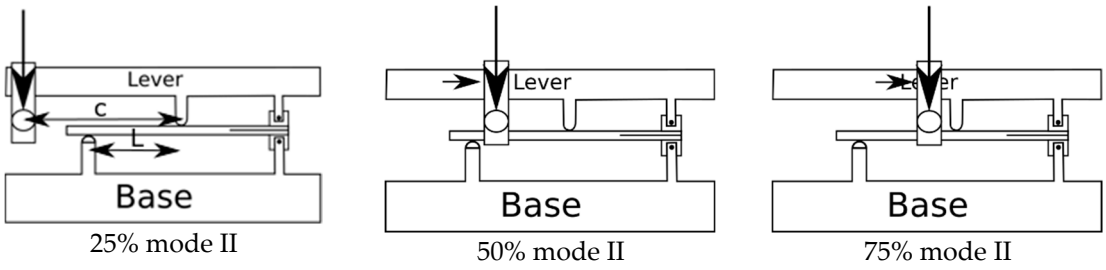

Figure 3. Different MMB test configurations.

The mode I and mode II energy release rates are calculated separately as follows:

$$G_I = \frac{12P^2(3c-L)^2}{16b^2h^3L^2E_{1f}}(a+\chi h)^2 \tag{4}$$

$$G_{II} = \frac{19P^2(c+L)^2}{16b^2h^3L^2E_{1f}}(a+0.42\chi h)^2, \text{ with} \tag{5}$$

$$\chi \equiv \sqrt{\frac{E_{11}}{11G_{13}}\left(3-2\left(\frac{\Gamma}{1+\Gamma}\right)\right)} \text{ and } \Gamma \equiv 1.18\frac{\sqrt{E_{11}E_{22}}}{G_{13}} \tag{6}$$

In all these equations, in addition to the terms from previous equations and starting from the calculation of the mode I energy release rate G_I, c is the lever length, as shown in Figure 3 in mm, L is the half-span length, also shown in Figure 3 in mm, χ is the crack length correction factor, E_{11} is the longitudinal modulus measured experimentally at 97 GPa, E_{22} is the transverse modulus, measured experimentally to be 7.0 GPa and, finally, G_{13} is the shear modulus estimated to be 8.5 GPa. As for the previous test methods, the loading rate was 1 mm/min. Crack length was also measured using a camera and by painting one of the specimen's edges, together with numerical interpolation. The results from the MMB test are plotted as the total energy release rate $G = G_I + G_{II}$ versus the mode II contribution $\frac{G_{II}}{G}$, as suggested by Benzeggagh and Kenane [29]. In this study, three ratios of mode mixity were tested, corresponding to mode II percentages of 25, 50 and 75%.

Data were then fitted using the Benzeggagh–Kenane (B-K) criterion using the following equation:

$$G_T = G_{Ic} + \left(G_{II_C} - G_{I_C}\right)\left(\frac{G_{II}}{G}\right)^n \tag{7}$$

The parameter n of the B-K criterion was found using a least squares method. This parameter reflects the influence of the mode II loading on the global energy release rate. A higher value of n indicates that the mode II plays a greater role in the total energy release rate, but the value is only used as a material characterization parameter here.

In order to obtain reliable propagation values, a particular data reduction method was developed to process the R-curves (G versus crack length). The curve was first limited to only include data for crack increases of 0.1 mm. This allowed a global average to be calculated without artificially weighting the value. Then, peaks and troughs were automatically retrieved from the curve using an Excel® routine. An example of an R-curve with peaks and troughs is shown in Figure 4.

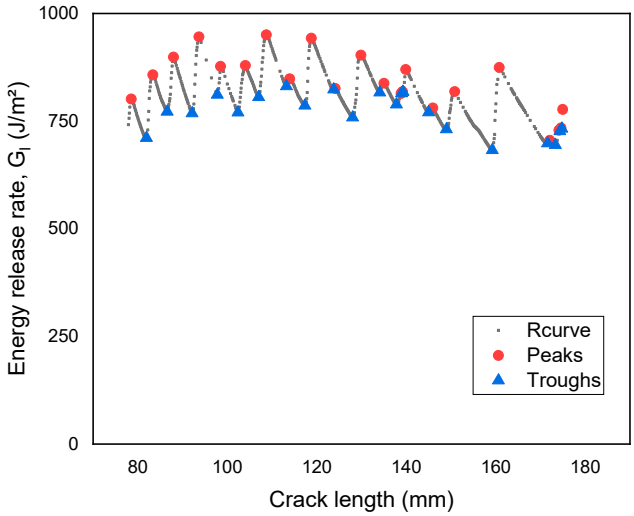

Figure 4. Example of peaks and troughs retrieved from R-curve.

4. Results

4.1. Water Uptake

Figure 5 shows weight gain measurements for three mode I fracture test specimens, first for immersion to saturation in seawater at 60 °C and then for drying.

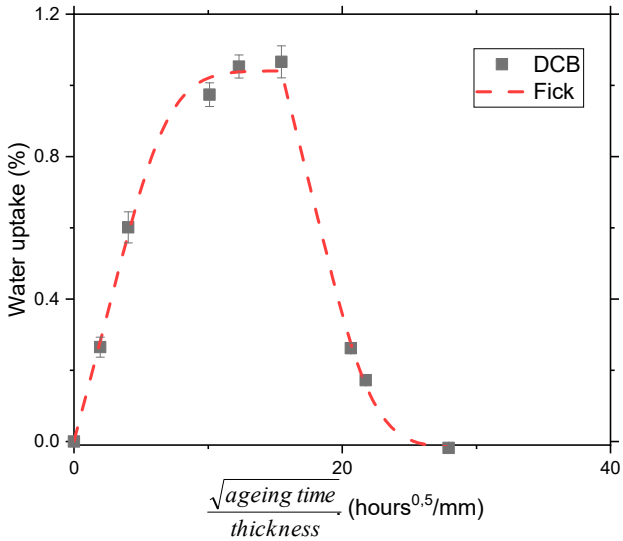

Figure 5. Mode I specimen water uptake after aging in natural seawater at 60°C and drying at 60 °C.

This plot shows similar weight gain kinetics and saturation values to those of the square coupon samples (Figure 2) and indicates that the weight gain is reversible after drying.

4.2. Mode I Fracture

Figure 6 shows examples of load-displacement plots for unaged mode I and mode II specimens. The propagation is unstable. One can note the difference in load level required to propagate cracks for these two tests. For both, precracked initial crack length was around 70 mm and final crack length was around 110 mm for DCB and 130 mm for ELS.

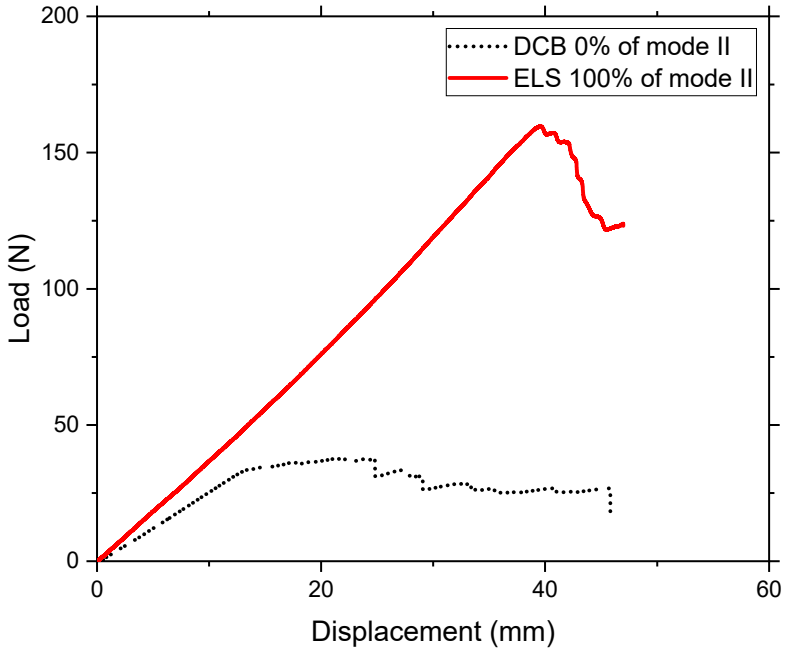

Figure 6. Load-displacement plot, unaged mode I and mode II specimens.

An example of an R-curve (G_I versus crack length) for the composite under mode I loading in the three ageing conditions is shown in Figure 7. The trend of the R-curves is globally stable with crack length but one can clearly observe local peaks and troughs for the unaged material, often attributed to a stick-slip behavior. This has been explained previously in terms of a local crack blunting mechanism [30]. Five specimens were tested for each condition, but only four results were retained for the saturated and dried conditions due to experimental incidents (debonding of load blocks during the tests). The dried condition showed less variability in propagation compared to the two other ageing conditions. These values are summarized with initiation values in Table 2.

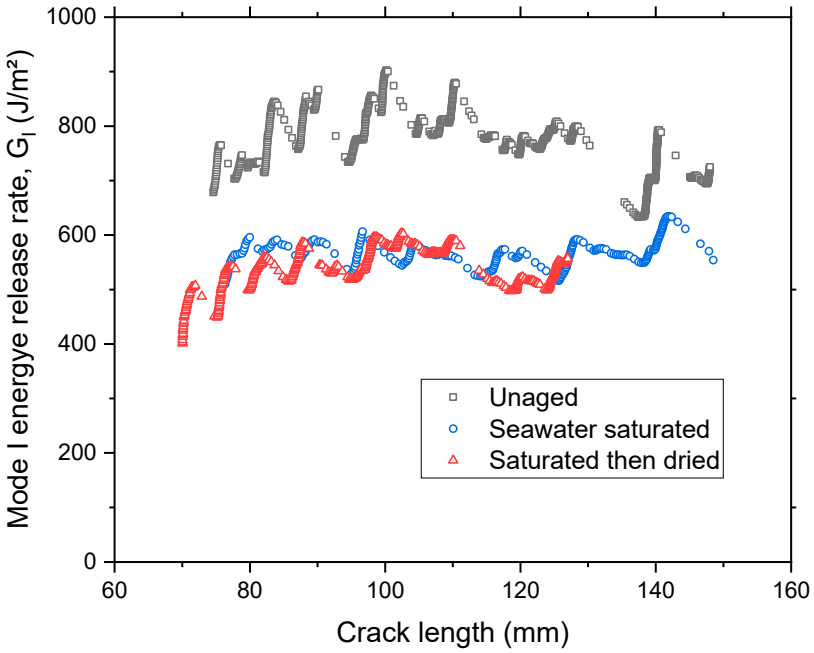

Figure 7. Examples of R-curves for unaged, seawater saturated and saturated then dried mode I specimens.

Table 2. Initiation and propagation values for all mode I tests; mean (standard deviation) values in J/m^2 (arrows show trends compared to the previous ageing condition).

	Initiation from Film		Initiation from Precrack		Propagation		
Criterion	**NL**	**5%/Max.**	**NL**	**5%/Max**	**Mean Entire R-Curve**	**Peak**	**Valley**
Unaged, Dry	281 (55)	353 (19)	388 (80)	527 (79)	799 (89)	835 (93)	722 (77)
Saturated	↘246 (67)	↘293 (25)	↘277 (13)	↘432 (11)	↘600 (105)	↘616 (96)	↘597 (102)
Re-dried after saturation	↘219 (13)	↘272 (48)	↗355 (60)	↗468 (42)	↘564 (57)	↘570 (55)	↘559 (55)

There is some scatter, but it is possible to obtain an average propagation energy release rate of around 800 J/m^2 for unaged, 600 J/m^2 for seawater saturated and 560 J/m^2 for re-dried specimens. Overall, for all the fracture parameters calculated from mode I loading tests, saturation in seawater at 60 °C reduces mode I fracture resistance by around 30% and this change is not reversible after drying.

4.3. Mode II Fracture

Figure 8 shows examples of the R-curves (G_{II} versus crack length) for the composite under mode II loading. One can see the difference in shape of the R-curves compared to those of the DCB test. For mode II, the R-curves are smooth compared to the mode I propagation; therefore, no "Peak" nor "Trough" values can be calculated. It is also worth noting the higher values of energies involved in mode II delamination compared to mode I. Table 3 shows initiation and propagation values for all mode II tests.

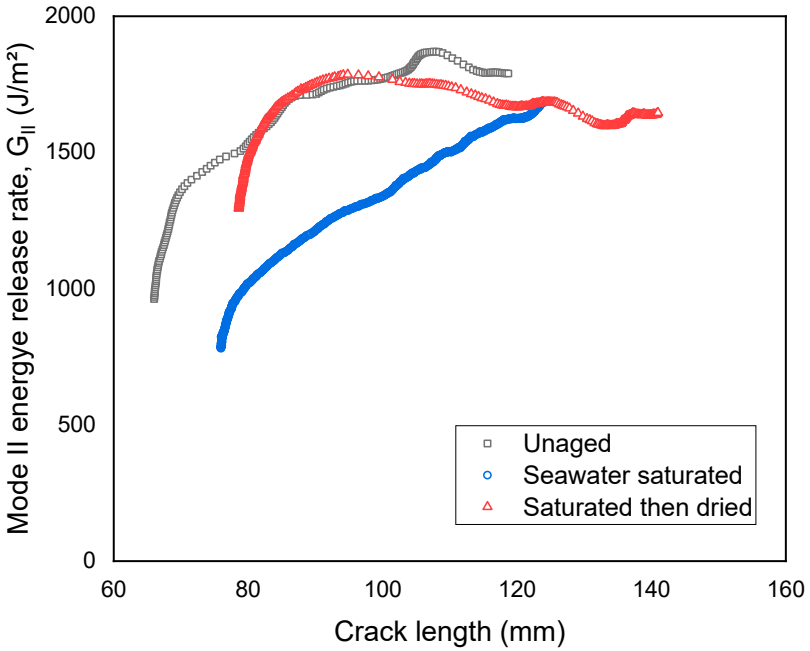

Figure 8. Examples of R-curves for unaged, saturated and saturated then dried mode II specimens.

Table 3. Initiation and propagation values for all mode II tests; mean (standard deviation) values in J/m^2 (arrows show trends compared to the previous ageing condition).

	Initiation from Film		**Initiation from Precrack**		**Propagation**
Criterion	NL	5%/Max.	NL	5%/Max	Mean Entire R-Curve
Unaged, Dry	738 (234)	1046 (216)	1078 (316)	1455 (253)	1790 (410)
Saturated	↘562 (97)	↘713 (93)	↘1032 (176)	↘1255 (261)	↘1378 (388)
Re-dried after saturation	↗728 (124)	↗958 (80)	↘993 (163)	↗1374 (236)	↗1475 (255)

There is a trend showing a decrease in G_{II} after seawater ageing, but there is significant variability in the results and differences are within one standard deviation. This will be discussed further below. Values after drying tend to increase but do not return to unaged values. As with mode I, the standard deviation seems to be lower in the final dried ageing condition.

4.4. Mixed Mode Fracture

Figure 9 shows an example of the load–displacement plots from mixed mode MMB tests for the three mode ratios. Here, again, the increasing mode II contribution corresponds to higher loads during the test.

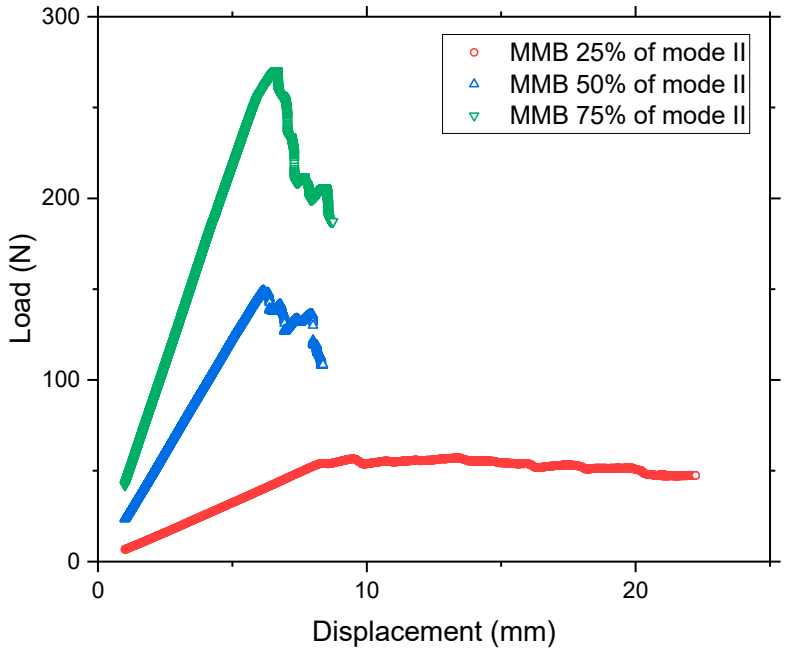

Figure 9. Load-displacement plots, 3 mixed mode ratios.

The R-curves of the MMB tests at the two ageing conditions and for the three mode mixities is shown in Figure 10.

These plots reveal one of the difficulties with MMB tests, namely that the propagation length is quite short (20–30 mm at most) compared to the mode I tests. As a result, the R-curves tend to increase and do not reach a plateau value. In this case, it is interesting to compare initiation values. For the 75% mode II case, the R-curves are more stable. Table 4 shows these initiation and propagation values for the three mixed mode tests.

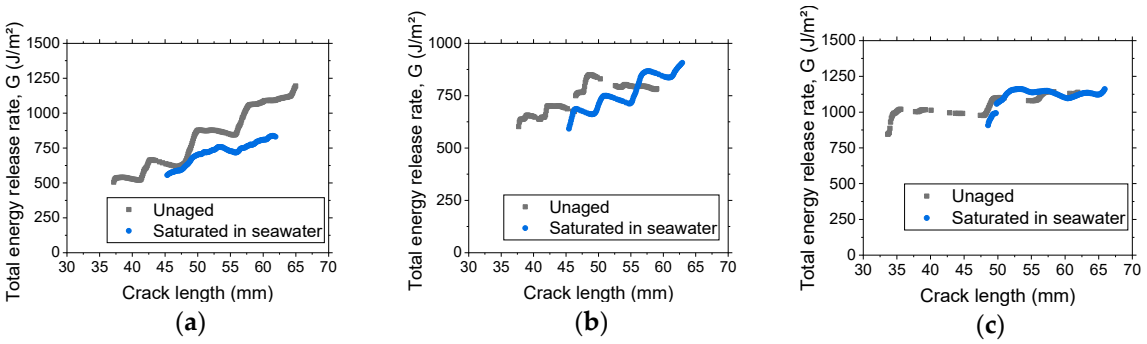

Figure 10. Examples of R-curves for unaged, and saturated mixed mode specimens, (25 (**a**), 50 (**b**) and 75% (**c**) of mode II).

Table 4. Initiation and propagation values for mixed mode (I/II) tests.

25% Mode II	**Initiation from Film**		**Initiation from Precrack**		**Propagation**		
Criterion	NL	5%/Max.	NL	5%/Max	Global mean	Peak	Valley
Unaged, Dry	348 (134)	449 (148)	373 (163)	473 (192)	818 (315)	913 (339)	859 (333)
Saturated	↘174 (48)	↘271 (46)	↘280 (29)	↘416 (33)	↘712 (183)	↘764 (175)	↘728 (168)
50% Mode II	**Initiation from Film**		**Initiation from Precrack**		**Propagation**		
Criterion	NL	5%/Max.	NL	5%/Max	Global mean	Peak	Valley
Unaged, Dry	544 (36)	752 (52)	517 (48)	670 (132)	795 (134)	813 (148)	780 (148)
Saturated	↘303 (52)	↘403 (40)	↘421 (58)	↘576 (66)	↘708 (134)	↘748 (139)	↘706 (143)
75% Mode II	**Initiation from Film**		**Initiation from Precrack**		**Propagation**		
Criterion	NL	5%/Max.	NL	5%/Max	Global mean	Peak	Valley
Unaged, Dry	591 (162)	783 (135)	562 (109)	759 (111)	942 (113)	1020 (112)	935 (97)
Saturated	↘491 (13)	↘716 (75)	↗676 (141)	↗867 (110)	↗1063 (144)	↗1134 (111)	↗1093 (88)

Once again, the overall trend indicates a decrease due to seawater ageing for the mode I dominated fractures, but for the 75% mode II fracture, saturation of specimens tends to result in a slightly higher energy release rate.

5. Discussion

- **Influence of an accelerated wet ageing protocol on mixed mode failure criteria**

The influence of seawater ageing on initiation and propagation values of strain energy release rate is shown in Figure 11.

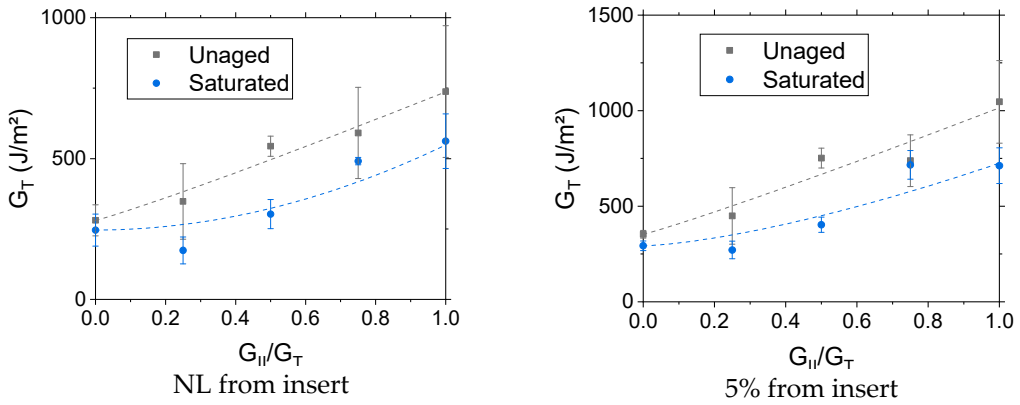

Figure 11. *Cont.*

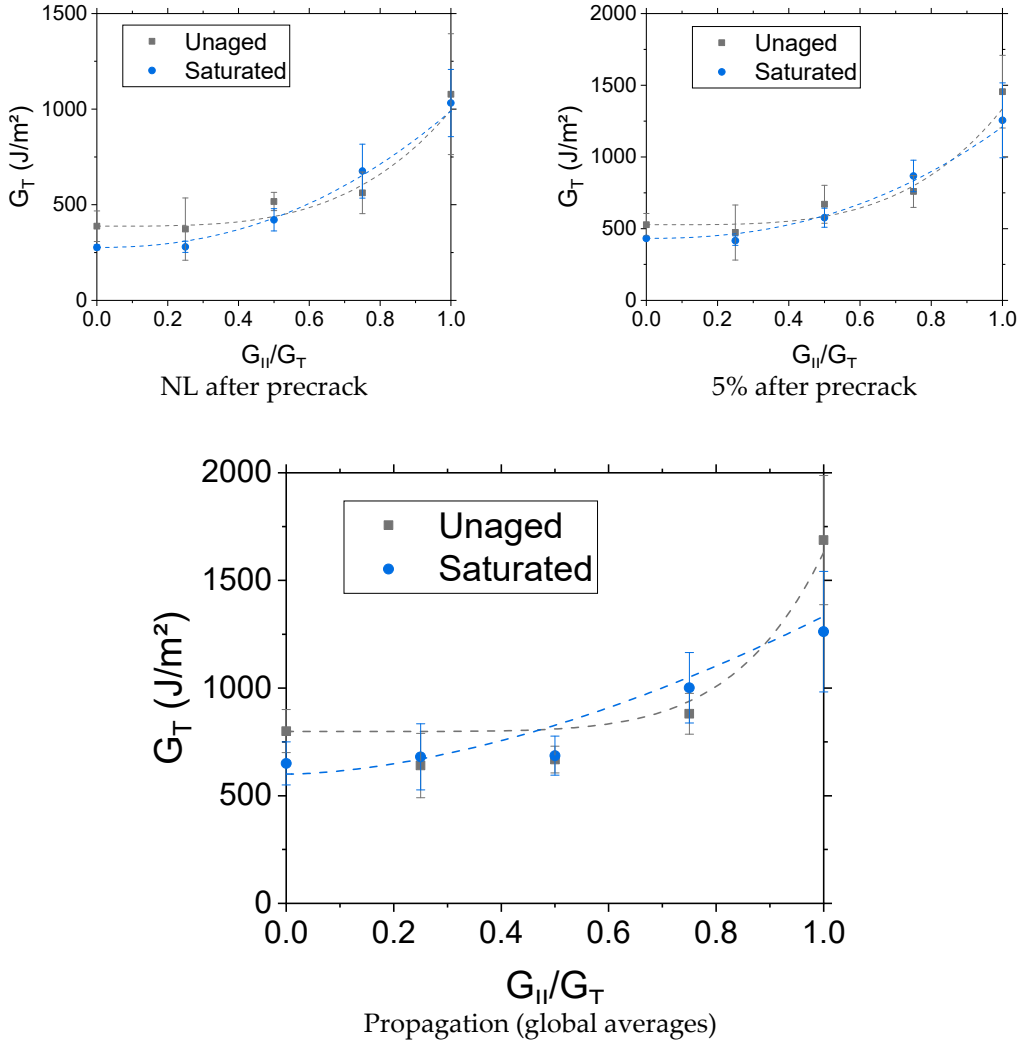

Figure 11. Summary of results for initiation and propagation; lines are B-K fits.

First, it should be noted that the interlaminar fracture toughness values measured here are in a similar range to published values for marine carbon/epoxy specimens. For example, Baral et al. studied a range of high modulus composites used for racing yachts and found mode I initiation values in the range of 200–300 J/m^2 with propagation values up to 700 J/m^2 [31]. Mode II fracture energies for carbon/epoxies are typically three times higher than those found under mode I loading [32], with this ratio decreasing as mode I toughness increases.

Second, it may be noted that, globally, the influence of seawater saturation on the interlaminar fracture behavior of this carbon/epoxy composite is small given the error bars. The results have been analyzed using the Benzeggagh and Kenane representation (B-K) [29] and this provides a reasonably good fit to all data. The n-parameters obtained for the unaged material are compared with published values for a glass/epoxy and carbon/peek composite in Table 5. It is apparent that, for values measured from the insert film, there is a stronger influence of the mode II loading component after saturation, while, for values from a precrack and propagation values, this mode II influence is lower after saturation. No published values were found for this parameter after seawater saturation.

Table 5. Mixed mode B-K failure criteria parameter n.

n	Unaged	Seawater Saturated
NL film	1.085	↗1.972
5% film	1.079	↗1.458
NL precrack	3.588	↘2.215
5% precrack	3.793	↘2.300
Propagation	6.189	↘1.693
Glass/epoxy [29]	2.6	-
Carbon/PEEK [31]	2.284	-

- **Influence of physical ageing**

An important feature of the values of G_{Ic} after drying, shown in Table 2, and, to a lesser extent, mode II values (Table 3) is that they did not return to their initial unaged values, even though the water ingress was shown to be reversible (Figure 5). This suggests that the material has undergone some permanent changes. This may indicate permanent damage, in the form of fiber/matrix debonding. Scanning electron microscopy was performed on unaged and aged fracture surfaces, but no significant differences were noted (no evidence of cleaner fibers after ageing, for example), so images are not shown here. Another possible explanation, which has received little attention in the published literature to date, is that the material undergoes physical ageing during immersion and drying at 60 °C. Physical ageing (PA) is a gradual change towards a more stable state of a polymer which has undergone rapid cooling below its glass transition temperature. Heating to a temperature close to the Tg will accelerate this change, related to molecular rearrangements, and it is usually accompanied by a reduction in tensile strain at failure [33,34]. At lower temperatures, these changes will take longer. Previous work on this same epoxy resin without fiber reinforcement [35] showed such an embrittlement with physical ageing, with faster property changes at closer to Tg temperatures. This is a reversible process; complete recovery of initial properties was noted after rejuvenation, a thermal treatment above Tg.

In order to examine the hypothesis that PA occurred during immersion and drying, a second series of mode I and mode II tests was performed on samples which had either been rejuvenated before testing or placed in conditions encouraging PA. The rejuvenation procedure involved heating above the Tg for a short time, then quenching in 15 °C water (samples were placed in sealed bags to prevent any contact with the water). Physically aged specimens were heated in an oven at 60 °C for 3 weeks. This temperature and ageing time were found in the previous study on the resin [35] and were estimated to provide conditions for a relatively complete PA. Tables 6 and 7 show the results from the mode I and mode II fracture tests on these conditioned specimens.

Table 6. Influence of physical ageing on energy release rate in mode I.

	Initiation from Film		Initiation from Precrack		Propagation		
Criterion	**NL**	**5%/Max.**	**NL**	**5%/Max**	**Mean Entire R-Curve**	**Peak**	**Valley**
Rejuvenated	190 (57)	359 (120)	497 (21)	816 (14)	800 (103)	832 (98)	744 (76)
Physically aged in air	↔189 (57)	↘295 (80)	↘386 (77)	↘632 (95)	↘621 (57)	↘645 (57)	↘603 (53)

These results indicate that PA does have an impact on the energy release rate for both mode I and mode II for the majority of the initiation and propagation values. The energy release rates decrease with PA. The reduction is significant for mode I and less important for mode II loading. The magnitude is similar to the reductions noted after seawater ageing, suggesting that PA, due to the increase in temperature imposed by the accelerated ageing protocol, is the main mechanism acting to reduce delamination resistance here.

Table 7. Influence of physical ageing on energy release rate in mode II.

	Initiation from Film		Initiation from Precrack		Propagation
Criterion	**NL**	**5%/Max.**	**NL**	**5%/Max**	**Mean Entire R-Curve**
Rejuvenated	546 (90)	720 (95)	683 (131)	971 (116)	1275 (121)
Physically aged in air	↗584 (51)	↗768 (24)	↘596 (20)	↘912 (23)	↘1119 (98)

From this complementary study, it is clear that accelerated ageing of carbon/epoxy composites with low Tg resin can lead to complex test results. Nevertheless, it should be emphasized that the overall effect is limited; once it has been quantified, it is easy to design structures so that early failure can be avoided, at least under quasi-static loadings.

- **Applicability of test results**

The data shown in this paper were analyzed using an approach based on a number of assumptions. First, the equations employed assume linear elastic fracture mechanics. The specimens were dimensioned following the standards to achieve this, and unloading indicated no permanent residual displacement which would have indicated widespread damage in the specimen arms.

Second, physical ageing effects due to the extended period at 60 °C also contribute to the final value and result in a lower delamination resistance. This contribution will also occur if ageing and drying are performed at lower temperatures and in real marine structures but will require longer times to appear. The ageing protocol adopted here thus provides a conservative value of delamination resistance. Further tests would be required at different times and temperatures to establish the physical ageing kinetics in these composites, as was done for the resin alone previously [35]. Given the fact that water ingress can also reduce the Tg of epoxy matrices due to plasticization [36–38], physical ageing could also finally appear at ageing temperatures considered as too far from Tg to happen in relevant timescales.

Third, there has been considerable discussion in the published literature on the values to be used in modeling. Tests for each loading condition yield several results here, with initiation from an implanted film, from a precrack and average values for a propagating crack. In addition, different initiation criteria and data analyses are provided by the standard test procedures. In the present case, up to seven values are defined. This multiplicity of values arose due to both the integration of different national protocols into one ISO document and the need to highlight the specimen geometry dependence of propagation values caused by fiber bridging and multiple cracking. Given that the same specimen geometry was used throughout this study, it is interesting to compare the ratio of results from five values before and after water ageing. Figure 12 shows these ratios.

There is a change in the influence of the water ageing protocol as the mode II contribution increases, with the effect becoming positive at high mode II ratio, but the results from the ELS test are in contradiction with this trend.

Pure mode II tests show considerably higher scatter than those from 75% mode II, which makes it difficult to formulate conclusions regarding ageing effects. Development of a standard test to measure mode II delamination resistance has proved difficult. Initially, the end notch flexure specimen appeared suitable [39,40], but the unstable nature of propagation during this test was not satisfactory. Tests promoting stable propagation, using 4-point ENF (End Notched Flexure) [41] and end loaded split specimens such as those tested here [13] were therefore preferred as they allow multiple values to be measured on each specimen. However, these and all mode II configurations suffer from the influence of friction between the propagating crack surfaces. As a result, some authors have questioned whether a pure mode II test is possible [42]. For ageing studies, this also introduces an additional unknown factor: the influence of water in the saturated material on friction effects.

An alternative pragmatic approach to examining the influence of in-plane shear loading is to apply a mode II dominated mixed mode test, as this involves a small opening component which limits

crack surface contact. In the present case, such an approach appears more consistent with mixed mode results for lower mode II loads. If propagation results are needed and the short MMB propagation distance is a constraint, some additional tests with an alternative fixture such as the asymmetric DCB proposed by Vanderkley [43] may be useful.

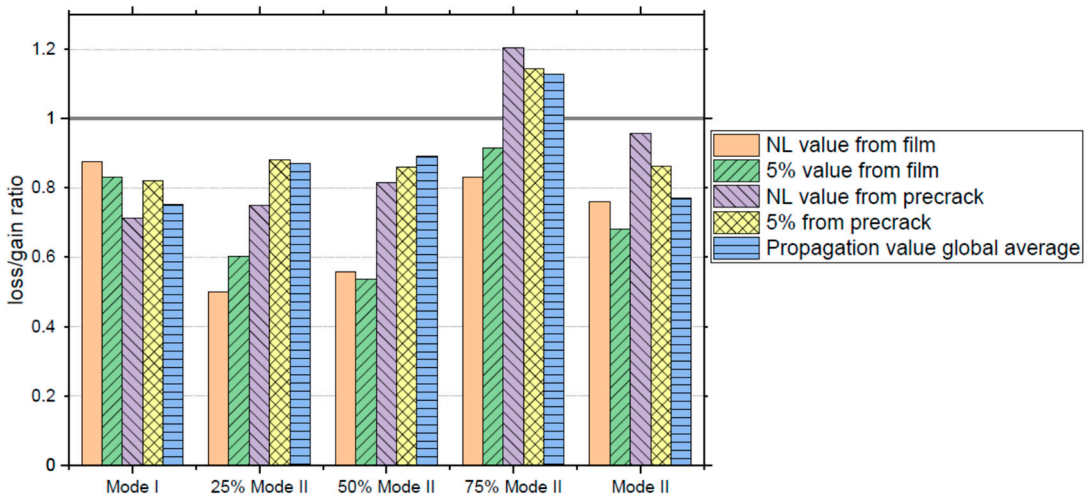

Figure 12. Ratios of water saturated/unaged fracture resistance values.

6. Conclusions

This paper presents a new set of results from a detailed study of the influence of seawater immersion on the interlaminar fracture resistance of a carbon/epoxy composite. It is shown that care is needed to dissociate changes due to water ingress from those associated with physical ageing due to polymer chain reorganization. The latter tend to reduce fracture toughness; the mechanism is slow at temperatures well below the glass transition temperature, but when raised temperatures are used to accelerate water ingress, these will also accelerate physical ageing. Specific tests were performed to quantify the latter and it appears to be the main mechanism contributing to changes in fracture resistance with this accelerated ageing protocol. It is therefore strongly recommended that for marine composites subjected to ageing at temperatures approaching their Tg separate tests be performed to dissociate these two effects.

However, even accounting for this second ageing mechanism, the interlaminar fracture behavior of this composite is quite stable, indicating that it is a good contender for marine applications where out-of-plane loading occurs.

Author Contributions: Funding acquisition, P.D. and B.H.; investigation, A.L.G.-G.; methodology, A.L.G.-G., P.D., P.-Y.L.G. and B.H.; supervision, P.D. and P.-Y.L.G.; writing—original draft, A.L.G.-G.; writing—review and editing, P.D., P.-Y.L.G. and B.H. All authors have read and agreed to the published version of the manuscript.

Funding: This research was funded by DGA and IFREMER.

Acknowledgments: The authors are grateful to the DGA and IFREMER for co-funding this study. The technical assistance of colleagues at the IFREMER Centre (Luc Riou, Mickael Premel-Cabic, Nicolas Lacotte and Mael Arhant) is gratefully acknowledged.

Conflicts of Interest: The authors declare no conflict of interest.

References

1. Smith, C.S. *Design of Marine Structures in Composite Materials*; Elsevier Applied Science: London, UK, 1990.
2. Graham-Jones, J.; Summerscales, J. (Eds.) *Marine Applications of Advanced Fibre-reinforced Composites*; Woodhead Publishing: Cambridge, UK, 2016.
3. Marsh, G. Fifty years of reinforced plastic boats. *Reinf. Plast.* **2006**, *50*, 16–19. [CrossRef]

4. Ochoa, O.; Salama, M.M. Offshore composites: Transition barriers to an enabling technology. *Compos. Sci. Technol.* **2005**, *65*, 2588–2596. [CrossRef]
5. Melot, D. Present and Future Composites Requirements for the Offshore Oil and Gas Industry. In *Durability of Composites in a Marine Environment 2*; Davies, P., Rajapakse, Y.D.S., Eds.; Springer: Dordrecht, The Netherlands, 2017; pp. 151–172.
6. Bir, G.S.; Lawson, M.; Li, Y. Structural Design of a Horizontal-Axis Tidal Current Turbine Composite Blade. In Proceedings of the ASME 30th International Conference on Ocean, Offshore, and Arctic Engineering, Rotterdam, The Netherlands, 19–24 June 2011.
7. Ennis, B.L.; Kelley, C.L.; Naughton, B.T.; Norris, R.E.; Das, S.; Lee, D.; Miller, D.A. *Optimized Carbon Fiber Composites in Wind Turbine Blade Design*; SANDIA Report SAND2019-14173; Sandia Labs: Albuquerque, NM, USA, November 2019.
8. Friedrich, K. (Ed.) *Application of Fracture Mechanics to Composite Materials*; Elsevier: Amsterdam, The Netherlands, 1989.
9. Moore, D.R.; Williams, J.G.; Pavan, A. *Fracture Mechanics Testing Methods for Polymers, Adhesives and Composites*; Elsevier: Amsterdam, The Netherlands, 2001.
10. ISO 15024:2001. *Fibre-Reinforced Plastic Composites—Determination of Mode I Interlaminar Fracture Toughness, GIC, for Unidirectionally Reinforced Materials*; ISO: Geneva, Switzerland, 2001.
11. Davies, P.; Sims, G.D.; Blackman, B.R.K.; Brunner, A.J.; Kageyama, K.; Hojo, M.; Tanaka, K.; Murri, G.; Rousseau, C.; Gieseke, B.; et al. Comparison of test configurations for the determination of GIIc: Results from an international round robin. *Plast. Rubber Compos.* **1999**, *28*, 432–437. [CrossRef]
12. Davidson, B.D.; Sun, X. Effects of Friction, Geometry, and Fixture Compliance on the Perceived Toughness from Three-and Four-Point Bend End-Notched Flexure Tests. *J. Reinf. Plast. Compos.* **2005**, *24*, 1611–1628. [CrossRef]
13. ISO 15114:2014. *Fibre-Reinforced Plastic Composites—Determination of the Mode II Fracture Resistance for Unidirectionally Reinforced Materials Using the Calibrated End-Loaded Split (C-ELS) Test and an Effective Crack Length Approach*; ISO: Geneva, Switzerland, 2014.
14. Reeder, J.; Crews, J.J. The mixed-mode bending method for delamination testing. *AIAA J.* **1989**, *28*, 1270–1276. [CrossRef]
15. ASTM D6671. *Standard Test Method for Mixed Mode I-Mode II Interlaminar Fracture Toughness of Unidirectional Fiber Reinforced Polymer Matrix Composites*; ASTM: Philadelphia, PA, USA, 2001.
16. Alfano, G.; Crisfield, M.A. Finite element interface models for the delamination analysis of laminated composites: Mechanical and computational issues. *Int. J. Numer. Methods Eng.* **2001**, *50*, 1701–1736. [CrossRef]
17. Blackman, B.R.K.; Hadavinia, H.; Kinloch, A.J.; Williams, J.G. The use of a cohesive zone model to study the fracture of fibre composites and adhesively-bonded joints. *Int. J. Fract.* **2003**, *119*, 25–46. [CrossRef]
18. Marom, G. Environmental Effects on Fracture Mechanical Properties of Polymer Composites. In *Application of Fracture Mechanics to Composite Materials*; Friedrich, K., Ed.; Elsevier: Amsterdam, The Netherlands, 1989; pp. 397–424.
19. Thomson, K.W.; Broutman, L.J. The effect of water on the fracture surface energy of fiber-reinforced composite materials. *Polym. Compos.* **1982**, *3*, 113–117. [CrossRef]
20. Russell, A.; Street, K. Moisture and Temperature Effects on the Mixed-Mode Delamination Fracture of Unidirectional Graphite/Epoxy. In *Delamination and Debonding of Materials*; ASTM STP 876; Johnson, W., Ed.; ASTM International: Philadelphia, PA, USA, 1985; pp. 349–370.
21. Garg, A.; Ishai, O. Hygrothermal influence on delamination behavior of graphite/epoxy laminates. *Eng. Fract. Mech.* **1985**, *22*, 413–427. [CrossRef]
22. Selzer, R.; Friedrich, K. Influence of water up-take on interlaminar fracture properties of carbon fibre-reinforced polymer composites. *J. Mater. Sci.* **1995**, *30*, 334–338. [CrossRef]
23. Zhao, S.; Gaedke, M. Moisture effects on Mode II delamination behavior of carbon/epoxy composites. *Adv. Compos. Mater.* **1996**, *5*, 291–307. [CrossRef]
24. Chou, I. Effect of fiber orientation and moisture absorption on the interlaminar fracture toughness of CFRP laminates. *Adv. Compos. Mater.* **1998**, *7*, 377–394. [CrossRef]
25. Asp, L.E. The effects of moisture and temperature on the interlaminar delamination toughness of a carbon/epoxy composite. *Compos. Sci. Technol.* **1998**, *58*, 967–977. [CrossRef]

26. Landry, B.; La Plante, G.; Le blanc, L.R. Environmental effects on mode II fatigue delamination growth in an aerospace grade carbon/epoxy composite. *Compos. Part A Appl. Sci. Manuf.* **2012**, *43*, 475–485. [CrossRef]
27. Couture, A.; Laliberte, J.; Li, C. Mode I Fracture Toughness of Aerospace Polymer Composites Exposed to Fresh and Salt Water. *Chem. Mater. Eng.* **2013**, *1*, 8–17.
28. Le Blanc, L.; La Plante, G.; Li, C. Moisture effects on mixed-mode delamination of carbon/epoxy composites, in Design, Manufacturing and Applications of Composites. In *Proceedings of the Tenth Joint Canada-Japan Workshop on Composites, Vancouver, BC, Canada, 19–21 August 2014*; DEStech Publications, Inc.: Lancaster, PA, USA, 2015; p. 115.
29. Benzeggagh, M.; Kenane, M. Measurement of mixed-mode delamination fracture toughness of unidirectional glass/epoxy composites with mixed-mode bending apparatus. *Compos. Sci. Technol.* **1996**, *56*, 439–449. [CrossRef]
30. Kinloch, A.J.; Williams, J.G. Crack blunting mechanisms in polymers. *J. Mater. Sci.* **1980**, *15*, 987–996. [CrossRef]
31. Baral, N.; Davies, P.; Baley, C.; Bigourdan, B. Delamination behaviour of very high modulus carbon/epoxy marine composites. *Compos. Sci. Technol.* **2008**, *68*, 995–1007. [CrossRef]
32. Reeder, J.R. *An Examination of Mixed Mode Delamination Failure Criteria*; NASA Technical Memo 104210: Hampton, VA, USA, 1992.
33. Struik, L.C.E. *Physical Aging in Amorphous Polymers and Other Materials*; Elsevier: Amsterdam, The Netherlands, 1978.
34. Odegard, G.M.; Bandyopadhyay, A. Physical aging of epoxy polymers and their composites. *J. Polym. Sci. Part B Polym. Phys.* **2011**, *49*, 1695–1716. [CrossRef]
35. Le Guen-Geffroy, A.; Le Gac, P.-Y.; Habert, B.; Davies, P. Physical ageing of epoxy in a wet environment: Coupling between plasticization and physical ageing. *Polym. Degrad. Stab.* **2019**, *168*, 108947. [CrossRef]
36. El Yagoubi, J.; Lubineau, G.; Saghir, S.; Verdu, J.; Askari, A. Thermomechanical and hygroelastic properties of an epoxy system under humid and cold-warm cycling conditions. *Polym. Degrad. Stab.* **2014**, *99*, 146–155. [CrossRef]
37. Morgan, R.J.; O'Neal, J.E. The Durability of Epoxies. *Polym. Technol. Eng.* **1978**, *10*, 49–116. [CrossRef]
38. Nogueira, P.; Torres, A.; Abad, M.-J.; Cano, J.; Barral-Losada, L.F.; Ramírez, C.; López, J.; López-Bueno, I. Effect of water sorption on the structure and mechanical properties of an epoxy resin system. *J. Appl. Polym. Sci.* **2001**, *80*, 71–80. [CrossRef]
39. Barrett, J.; Foschi, R. Mode II stress-intensity factors for cracked wood beams. *Eng. Fract. Mech.* **1977**, *9*, 371–378. [CrossRef]
40. Carlsson, L.; Gillespie, J.; Pipes, R. On the Analysis and Design of the End Notched Flexure (ENF) Specimen for Mode II Testing. *J. Compos. Mater.* **1986**, *20*, 594–604. [CrossRef]
41. Martin, R.H.; Davidson, B. Mode II fracture toughness evaluation using a four point bend end notched flexure test. In *Proceedings of the 4th International Deformation and Fracture of Composites Conference (DFC4), London, UK, 24–26 March 1997*; Institute of Materials: London, UK, 1997; pp. 243–252.
42. O'Brien, T.K.; O'Brien, T. Composite Interlaminar Shear Fracture Toughness, GIIc: Shear Measurement or Sheer Myth? In *Composite Materials: Fatigue and Fracture*; Volume 7th, Bucinell, R., Ed.; ASTM STP 1330; ASTM International: West Conshohocken, PA, USA, 1998; pp. 3–18.
43. Vanderkley, P.S. Mode I-Mode II Delamination Fracture Toughness of a Unidirectional Graphite/Epoxy Composite. Master's Thesis, Texas A & M University, College Station, TX, USA, 1981.